Lossless intensity modulation in integrated photonics

Sunil Sandhu* **and Shanhui Fan**

Ginzton Laboratoy, Stanford University, Stanford, California 94305, USA

*centaur@stanford.edu

Abstract: We present a dynamical analysis of lossless intensity modulation in two different ring resonator geometries. In both geometries, we demonstrate modulation schemes that result in a symmetrical output with an infinite on/off ratio. The systems behave as lossless intensity modulators where the time-averaged output optical power is equal to the time-averaged input optical power.

OCIS codes: (230.0230) Optical devices; (140.4780) Optical resonators; (350.4238) Nanophotonics and photonic crystal.

References and links

1. G. T. Reed, G. Mashanovich, F. Y. Gardes, and D. J. Thomson, "Silicon optical modulators," Nat. Photonics **4**, 518–526 (2010).
2. A. Liu, R. Jones, L. Liao, D. Samara-Rubio1, D. Rubin, O. Cohen, R. Nicolaescu, and M. Paniccia, "A high-speed silicon optical modulator based on a metal-oxide-semiconductor capacitor," Nature **427**, 615–618 (2004).
3. L. Liao, D. Samara-Rubio, M. Morse, A. Liu, D. Hodge, D. Rubin, U. Keil, and T. Franck, "High speed silicon Mach-Zehnder modulator," Opt. Express **13**, 3129–3135 (2005).
4. L. Liao, A. Liu, J. Basak, H. Nguyen, M. Paniccia, D. Rubin, Y. Chetrit, R. Cohen, and N. Izhaky, "40 Gbit/s silicon optical modulator for highspeed applications," Electron. Lett. **43**, 1196–1197 (2007).
5. A. Liu, L. Liao, D. Rubin, H. Nguyen, B. Ciftcioglu, Y. Chetrit, N. Izhaky, and M. Paniccia, "High-speed optical modulation based on carrier depletion in a silicon waveguide," Opt. Express **15**, 660–668 (2007).
6. X. Chen, Y.-S. Chen, Y. Zhao, W. Jiang, and R. T. Chen, "Capacitor-embedded 0.54 pj/bit silicon-slot photonic crystal waveguide modulator," Opt. Lett. **34**, 602–604 (2009).
7. H.-W. Chen, Y.-H. Kuo, and J. E. Bowers, "25 Gb/s hybrid silicon switch using a capacitively loaded traveling wave electrode," Opt. Express **18**, 1070–1075 (2010).
8. Q. Xu, B. Schmidt, S. Pradhan, and M. Lipson, "Micrometre-scale silicon electro-optic modulator," Nature **435**, 325–327 (2005).
9. D. M. Gill, M. Rasras, K.-Y. Tu, Y.-K. Chen, A. E. White, S. S. Patel, D. Carothers, A. Pomerene, R. Kamocsai, C. Hill, and J. Beattie, "Internal bandwidth equalization in a CMOS-compatible Si-ring modulator," IEEE Photon. Technol. Lett. **21**, 200–202 (2009).
10. T. Tanabe, K. Nishiguchi, E. Kuramochi, and M. Notomi, "Low power and fast electro-optic silicon modulator with lateral p-i-n embedded photonic crystal nanocavity," Opt. Express **17**, 22505–22513 (2009).
11. S. Manipatruni, K. Preston, L. Chen, and M. Lipson, "Ultra-low voltage, ultra-small mode volume silicon microring modulator," Opt. Express **18**, 18235–18242 (2010).
12. A. Yariv, "Critical coupling and its control in optical waveguide-ring resonator systems," IEEE Photon. Technol. Lett. **14**, 483–485 (2002).
13. W. D. Sacher and J. K. S. Poon, "Characteristics of microring resonators with waveguide-resonator coupling modulation," J. Lightwave Technol. **27**, 3800–3811 (2009).
14. T. Ye and X. Cai, "On power consumption of silicon-microring-based optical modulators," J. Lightwave Technol. **28**, 1615–1623 (2010).
15. Z. Pan, S. Chandel and C. Yu, "Ultrahigh-speed optical pulse generation using a phase modulator and two stages of delayed Mach-Zehnder interferometers," Opt. Eng. **46**, 075001 (2007).
16. C. Schmidt-Langhorst and H.-G. Weber, "Optical sampling techniques," J. Opt. Fiber Commun. Rep. **2**, 86–114 (2005).
17. W. D. Sacher and J. K. S. Poon, "Dynamics of microring resonator modulators," Opt. Express **16**, 15741–15753 (2008).

#156102 - $15.00 USD Received 4 Nov 2011; revised 20 Jan 2012; accepted 30 Jan 2012; published 7 Feb 2012

18. M. F. Yanik and S. Fan, "Stopping light all optically," Phys. Rev. Lett. **92**, 083901 (2004).
19. A. Taflove and S. C. Hagness, *Computational Electrodynamics: The Finite-Difference Time-Domain Method*, 3rd ed. (Artech House, 2005).
20. Q. Reed, P. Dong, and M. Lipson, "Breaking the delay-bandwidth limit in a photonic structure," Nat. Phys. **3**, 406–410 (2007).
21. M. Lipson, "Guiding, modulating, and emitting light on silicon-challenges and opportunities," J. Lightwave Technol. **23**, 4222 – 4238 (2005).
22. Q. Xu, "Silicon dual-ring modulator," Opt. Express **17**, 20783–20793 (2009).

1. Introduction

Integrated photonics has attracted a great deal of attention in recent years because of its potential to realize faster and less power-consuming photonic devices. One key required functionality in integrated photonics is optical modulation [1]. For this purpose, electro-optic intensity modulators have been experimentally demonstrated in a variety of geometries such as the Mach-Zehnder interferometer [2–7] and resonators [8–11]. In particular, micro-ring resonator modulators are attractive because of their potential to achieve compact, low power-consumption and high-speed modulation [1]. A common way of performing optical modulation in these previously studied geometries is by operating around a lossy state where the transmission through the system is near zero. For example, in systems consisting of a micro-ring coupled to a waveguide [12–14], optical modulation is usually performed by operating around the *critical coupling* state where the ring resonator's intrinsic loss rate is equal to its waveguide coupling rate. However, operation around such a lossy state can result in a significant loss of optical power in these modulation schemes.

In this paper, we propose an alternative mechanism that achieves *lossless* intensity modulation. As an illustration, we consider lossless resonant all-pass filters consisting of a waveguide side-coupled to either a single-ring resonator or coupled-ring resonators. For such a system, when we input into the waveguide a continuous-wave (CW) signal, the steady state transmission coefficient is always unity, independent of the resonance frequency or the coupling constants of the system. Nevertheless, we show that significant intensity modulation of the system output can be achieved when the system parameters such as the resonant frequencies are modulated at a rate comparable to the waveguide coupling rate. In fact, the modulation *on/off ratio*, defined as the ratio of the maximum to minimum output power, can be infinity. This system behaves as a lossless intensity modulator where the time-averaged output optical power is equal to the time-averaged input optical power. Thus, the peak power of the modulated output signal is in fact higher than the input CW signal peak power. We also show that in the case of a coupled-three-ring system, a clear symmetric output pulse shape can be generated by only modulating the ring resonance frequency. Examples of possible applications of our intensity modulation schemes include optical clock signal generation and optical sampling [15, 16].

2. Photon dynamics in a modulated system

The conventional way of describing optical intensity modulation is by imagining a device whose steady state transmission spectrum T varies as a function of some parameter x [Fig. 1(a)]. For example, in the simple case of a single-ring modulator [12–14] shown in Fig. 2(a), x can either be the ring's resonance frequency, its radiative loss rate or its waveguide coupling rate. At some operating frequency ω of the system, the steady state transmission spectrum has a value of $T_{\max}$ for some $x = x_1$ and a value of $T_{\min}$ for some $x = x_2$. Modulating x between x_1 and x_2 [Fig. 1(b)] at some frequency Ω then results in the intensity modulation of an input optical beam between the $T_{\max}$ state and the $T_{\min}$ state [Fig. 1(c)] at the same frequency Ω. If we return back to our example of the single-ring modulator [Fig. 2(a)], the modulation of x here can be

#156102 - $15.00 USD Received 4 Nov 2011; revised 20 Jan 2012; accepted 30 Jan 2012; published 7 Feb 2012

carried out such that the single-ring system is modulated between (i) the critical coupling state where $T = T_{\min} = 0$, and (ii) away from the critical coupling state where $T = T_{\max} \approx 1$.

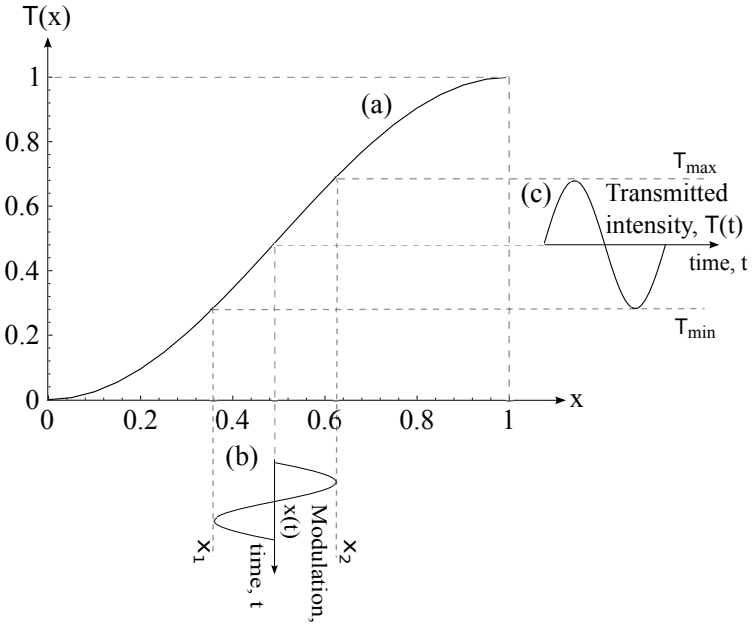

Fig. 1. Conventional way of describing intensity modulation which is only valid in the adiabatic regime: (a) transmission T of system as a function of some system parameter x, (b) modulation performed on x as a function of time, (c) resultant modulation of the system transmission T as a function of time.

It is important to realize that the schematic in Fig. 1 in fact is generally not an accurate description of the modulation process [14, 17]. In particular, this description implicitly assumes that the system responds instantaneously to any variation of the control parameter. However, such an instantaneous response is only valid in the adiabatic regime, when the modulation rate is far below the frequency scale of every important dynamic process of the system. A more accurate description of the modulation process requires the system dynamics to be taken into account [14, 17]. In the following two sections, we study the dynamics in two types of lossless resonant all-pass filters: (i) a single lossless ring resonator coupled to a waveguide, and (ii) a lossless coupled-three-ring resonator system coupled to a waveguide. We show that in both ring systems, when we input into the waveguide a CW signal at the system resonance frequency, a symmetric modulated output with infinite on/off ratio can be achieved by modulating some parameter in the system. Both systems behave as lossless intensity modulators where the time-averaged output optical power is equal to the time-averaged input optical power.

3. Single-ring system

We first consider the system shown in Fig. 2(a), consisting of a single ring coupled to a waveguide. The system can be described by the following coupled-mode theory (CMT) equations which have been previously shown to accurately describe the propagation of light in resonator

#156102 - $15.00 USD Received 4 Nov 2011; revised 20 Jan 2012; accepted 30 Jan 2012; published 7 Feb 2012

systems [18]:

$$\frac{da(t)}{dt} = j\,\omega_o\,a(t) - \left[\gamma_{coup}(t) + \gamma_{loss}\right] a(t) + j\,\sqrt{2\,\gamma_{coup}(t)}\,S_{in}(t)$$
$$S_{out}(t) = S_{in}(t) + j\,\sqrt{2\,\gamma_{coup}(t)}\,a(t). \tag{1}$$

Equation (1) describes the dynamics of the amplitude $a(t)$ of a ring resonator with the modal profile normalized such that $|a(t)|^2$ gives the energy in the mode. γ_{loss} is the ring resonator's amplitude-radiative loss rate, ω_o is the resonance frequency of the ring, and $S_{in}(t)$ $[S_{out}(t)]$ denotes the amplitude of the incoming [outgoing] wave in the waveguide with $|S_{in}(t)|^2$ and $|S_{out}(t)|^2$ giving the power in the waveguide mode. $\gamma_{coup}(t)$ is the time-dependent waveguide-ring amplitude coupling rate, related to the waveguide-ring power coupling ratio $1-\left|\exp\left(-\gamma_{coup}L/v\right)\right|^2$, where L =circumference of the ring and v = speed of light in the ring [12].

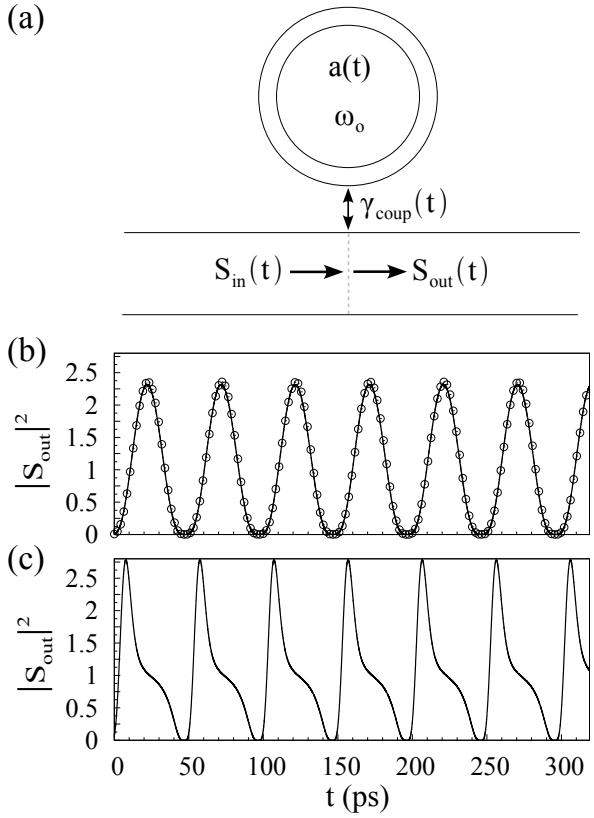

Fig. 2. Analysis of a single-ring system: (a) shows the schematic of the system where $a(t)$ is the ring modal amplitude, ω_o is the ring resonance frequency, $S_{in}(t)$ $[S_{out}(t)]$ are the incoming [outgoing] waveguide modal amplitude and $\gamma_{coup}(t)$ is the waveguide coupling rate. (b) and (c) show the system output power at $t \gg \frac{1}{\gamma_o}$ for a modulated coupling rate $\gamma_{coup}(t) = [0.069 + 0.025\sin(\Omega t)]\,\Omega$ and $\gamma_{coup}(t) = [6.43 + 2.92\sin(\Omega t)]\,\Omega$, respectively. In both (b) and (c), $\omega_o = 2\pi(193\,\text{THz})$, $S_{in} = \exp(j\omega_o t)$ and $\Omega = 2\pi(20\,\text{GHz})$. Circles in (b) show the output power using the approximation of Eq. (5).

In the case of a CW input $S_{in}(t) = \exp(j\,\omega t)$ and static coupling rate $\gamma_{coup}(t) = \gamma_{coup}$, the

#156102 - $15.00 USD Received 4 Nov 2011; revised 20 Jan 2012; accepted 30 Jan 2012; published 7 Feb 2012

transmission spectrum of the single-ring system is:

$$T(\omega) = \frac{S_{\text{out}}}{S_{\text{in}}} = \frac{\omega - \omega_{\text{o}} + j\left(\gamma_{\text{coup}} - \gamma_{\text{loss}}\right)}{\omega - \omega_{\text{o}} - j\left(\gamma_{\text{coup}} + \gamma_{\text{loss}}\right)}.$$

If we further assume the system is lossless (i.e. $\gamma_{\text{loss}} = 0$), the power transmission coefficient of the system is $|T(\omega)| = 1$ for all values of the coupling rate γ_{coup} and ring resonant frequency ω_{o}. Thus, the conventional description of intensity modulation in Fig. 1, which neglects the system dynamics, predicts that for the lossless ring system in Fig. 2, modulating any parameter at any modulation frequency will not result in the intensity modulation of an input optical beam.

We next examine the dynamical behavior of such a lossless ring system in the case of some time-dependent coupling rate $\gamma_{\text{coup}}(t)$ and CW input $S_{\text{in}}(t) = \exp(j\omega_o t)$ operating at the ring resonance frequency ω_o. From Eq. (1) we can derive the following analytical form of the system output:

$$S_{\text{out}}(t) = [1 + B(t)]\exp(j\omega_o t), \tag{2}$$

$$B(t) = j\sqrt{2\,\gamma_{\text{coup}}(t)}A(t), \tag{3}$$

$$A(t) = j\exp\left[-\int_0^t \gamma_{\text{coup}}(t')dt'\right]\int_0^t \sqrt{2\,\gamma_{\text{coup}}(\tau)}\,\exp\left[\int_0^\tau \gamma_{\text{coup}}(t')dt'\right]d\tau,$$

where the resonator amplitude $a(t) = A(t)\exp(j\omega_o t)$. The output $S_{\text{out}}(t)$ in Eq. (2) can be described as having a carrier frequency ω_o and an envelope $1 + B(t)$. The envelope results from the interference between a direct pathway of unity amplitude and an indirect pathway ring resonance assisted amplitude $B(t)$. The expression for $B(t)$ in Eq. (3) consists of integrals which contains *memory effects* as discussed in Ref. [17]. In the discussion below, we will demonstrate that these memory effects, which are significant only when the modulation is in the non-adiabatic regime, can give rise to lossless intensity modulation.

In the following examples, we specialize to a sinusoidal modulation of the waveguide coupling rate at a modulation frequency $\Omega = 2\pi(20\text{GHz})$:

$$\gamma_{\text{coup}}(t) = \gamma_{\text{o}} + \Delta\gamma\sin(\Omega t) \tag{4}$$

where γ_{o} is the mean coupling rate amplitude and $\Delta\gamma$ is the modulation amplitude. We numerically solve the single-ring system CMT equations [Eq. (1)] for the output $S_{\text{out}}(t)$. Figure 2(b) and 2(c) show the output power solutions at $t \gg \frac{1}{\gamma_{\text{o}}}$ for the cases $(\gamma_{\text{o}} = 0.069\Omega, \Delta\gamma = 0.025\Omega)$ and $(\gamma_{\text{o}} = 6.43\Omega, \Delta\gamma = 2.92\Omega)$, respectively. In both of these examples, the output power is modulated between a maximum amplitude state and a zero amplitude state (i.e. infinite on/off ratio) with a modulation frequency equivalent to the coupling rate modulation frequency $\Omega = 2\pi(20\text{GHz})$. Qualitatively, the maximum amplitude state in Fig. 2(b) and (c) occurs when there is constructive interference between the direct pathway amplitude and the resonance assisted indirect pathway amplitude in Eq. (2), while the zero amplitude state occurs when there is destructive interference between the pathways. In general, for any mean coupling rate amplitude $\gamma_{\text{o}} \ll \omega_{\text{o}}$ in Eq. (4), an infinite modulation on/off ratio can be achieved by an appropriate choice of the modulation amplitude $\Delta\gamma$.

We also see that a symmetrical output envelope is obtained in the weak coupling rate regime [Fig. 2(b)] where $\gamma_{\text{o}}, \Delta\gamma \ll \Omega$ and $\Delta\gamma < \gamma_{\text{o}}$ in Eq. (4). In this weak coupling rate regime, assuming a sinusoidal modulation of the coupling rate [Eq. (4)], the indirect pathway amplitude $B(t)$ in Eq. (3) at $t \gg \frac{1}{\gamma_{\text{o}}}$ can be approximated as:

$$B(t) \approx 2\sqrt{\frac{\gamma_{\text{coup}}(t)}{\gamma_{\text{o}}}}\left[\left(\frac{\Delta\gamma}{4\,\gamma_{\text{o}}}\right)^2 - 1\right]. \tag{5}$$

#156102 - $15.00 USD Received 4 Nov 2011; revised 20 Jan 2012; accepted 30 Jan 2012; published 7 Feb 2012

The circles in Fig. 2(b) shows a plot of the output power [Eq. (2)] using the approximation in Eq. (5). We see that there is excellent agreement with the unapproximated form (solid line) using Eq. (2) and (3). In Eq. (5), the resonator amplitude $a(t)$ within the original $B(t)$ expression [Eq. (3)] has been approximated by a constant. This constant energy within the resonator results in the modulation of the output envelope [Eq. (2)] being only driven by the $\sqrt{\gamma_{\text{coup}}(t)}$ term in Eq. (5). Hence, the output envelope is symmetrical in the weak coupling regime. Equation (5) also shows that for any mean coupling rate γ_0 in this weak coupling regime, an infinite on/off ratio can be achieved by using a modulation amplitude $\Delta\gamma \approx 0.73\gamma_0$.

On the other hand, strong coupling to the waveguide results in an asymmetrical output envelope [Fig. 2(c)]. For our sinusoidal modulation of the coupling rate in Eq. (4), the resonator amplitude $a(t)$ within the $B(t)$ expression [Eq. (3)] generally oscillates with the same periodicity as the coupling rate. However, in the strong coupling regime, the ratio of the variance to the mean value of $|a(t)|$ is significant. Hence, the modulation of the output envelope is driven by the product of a $\sqrt{\gamma_{\text{coup}}(t)}$ term and a non-constant resonator amplitude term in Eq. (3). In general, within a modulation cycle of the coupling rate, there is a time delay between the maximum points and between the minimum points of both these driving terms. Consequently, the output envelope is asymmetrical in the strong coupling regime.

We also emphasize that our above discussion of lossless optical modulation in either the weak coupling regime [Fig. 2(b)] or the strong coupling regime [Fig. 2(c)] is different as compared to the modulation schemes studied in Ref. [12–14]. In particular, the modulation schemes in Ref. [12–14] involve operation around the critical-coupling state which can result in a significant loss of optical power.

One common way of implementing the coupling modulation scheme in Fig. 2(a) is using either a composite interferometer [Fig. 3] or a simple directional coupler as outlined in Ref. [12]. However, such an implementation can result in a longer device length scale, and also higher power consumption [1, 14].

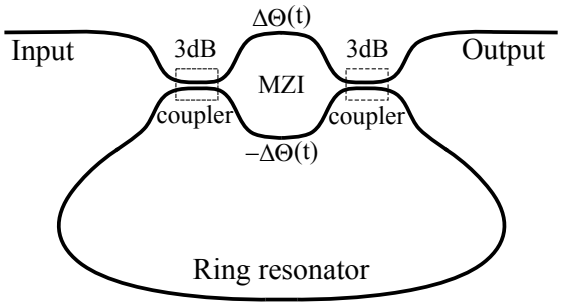

Fig. 3. Example implementation of waveguide coupling rate modulation in a single-ring system using a composite interferometer (CI) [12]. The CI consists of a Mach-Zehnder interferometer (MZI) sandwiched between two 3dB couplers. The MZI is driven in a push-pull configuration with modulated propagation phases $\pm\Delta\theta(t)$ that modulate the waveguide coupling rate.

4. Coupled-three-ring system

To overcome the length scale and power consumption issues associated with the structure shown in Fig. 3, we next introduce a modulation scheme based on coupled-ring resonators, where the system's *effective waveguide coupling rate* and, hence, output power can be modulated by modulating the resonance frequencies of a pair of resonators. In addition, we show that the resulting modulated output envelope of the system can be symmetrical with an infinite

#156102 - $15.00 USD Received 4 Nov 2011; revised 20 Jan 2012; accepted 30 Jan 2012; published 7 Feb 2012

on/off ratio. Our system (Fig. 4) consists of a pair of side ring resonators with modal amplitudes $p(t)$ and $q(t)$, coupled to a central ring resonator with modal amplitude $a(t)$. The coupling rate between each side ring and the central ring is κ, and the side rings are not directly coupled to each other. The central ring has a static resonance fequency ω_o while the two side rings have dynamic resonance frequencies $\omega_o + \Delta(t)$ and $\omega_o - \Delta(t)$, respectively. The central ring is coupled to a waveguide and this central-ring-waveguide part of the system has the same geometry as the single-ring system discussed in Section 3. The coupled-three-ring system can be described by the following CMT equations:

$$\begin{aligned}
\frac{da(t)}{dt} &= j\,\omega_o\,a(t) + j\,\kappa\,[p(t)+q(t)] - \left(\gamma_{coup}+\gamma_{loss}\right)a(t) + j\,\sqrt{2\,\gamma_{coup}}\,S_{in}(t)\\
\frac{dp(t)}{dt} &= j\,[\omega_o+\Delta(t)]\,p(t) + j\,\kappa\,a(t) - \gamma_{loss}\,p(t)\\
\frac{dq(t)}{dt} &= j\,[\omega_o-\Delta(t)]\,q(t) + j\,\kappa\,a(t) - \gamma_{loss}\,q(t)\\
S_{out}(t) &= S_{in}(t) + j\,\sqrt{2\,\gamma_{coup}}\,a(t).
\end{aligned} \tag{6}$$

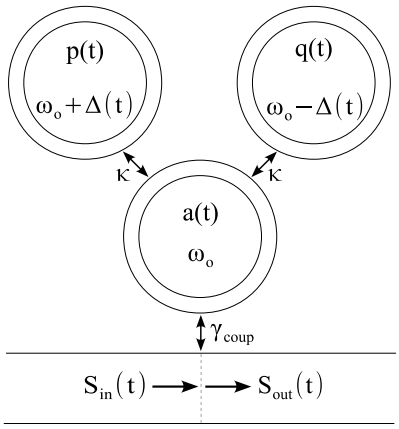

Fig. 4. Schematic of the coupled-three-ring system where $a(t)$, $p(t)$ and $q(t)$ are the rings' modal amplitudes, $S_{in}(t)$ [$S_{out}(t)$] is the incoming [outgoing] waveguide modal amplitude, κ is the inter-ring coupling rate, γ_{coup} is the waveguide coupling rate, ω_o is the central ring resonance frequency, and $\Delta(t)$ is the side ring detuning.

In the case of a CW input $S_{in}(t) = \exp(j\omega t)$ and a static side ring resonance frequency detuning $\Delta(t) = \Delta$, the transmission through the system is:

$$\begin{aligned}
T(\omega) &= \frac{S_{out}}{S_{in}} = \frac{\omega-\omega_o+y+j\left(\gamma_{coup}-\gamma_{loss}\right)}{\omega-\omega_o+y-j\left(\gamma_{coup}+\gamma_{loss}\right)}\\
y &= \frac{2\,\kappa^2\,(\omega-\omega_o-j\,\gamma_{loss})}{\Delta^2-(\omega-\omega_o-j\,\gamma_{loss})^2}.
\end{aligned}$$

If we further assume the system is lossless (i.e. $\gamma_{loss} = 0$), the absolute transmission of the system is $|T(\omega)| = 1$ for all values of the detuning Δ. On the other hand, the spectra of energy stored in each of the three resonators in Fig. 4 varies with Δ.

As a direct check of the CMT model [Eq. (6)], we simulate a coupled-three-ring system by solving Maxwells equations using the finite-difference time-domain (FDTD) method [19]. For

#156102 - $15.00 USD Received 4 Nov 2011; revised 20 Jan 2012; accepted 30 Jan 2012; published 7 Feb 2012

the FDTD simulations, the straight waveguide in Fig. 4 is chosen to have a width of $0.127\,\mu$m, such that the waveguide supports only a single mode in the $1.55\,\mu$m wavelength range. Each ring resonator waveguide has the same width as the straight waveguide, and a ring radius of $2\,\mu$m (measured from the center of the ring to its outer circumference). The center-to-center separation between the central ring and the straight waveguide is $2.417\,\mu$m while the center-to-center separation between the central ring and each side ring is $4.653\,\mu$m. The center-to-center separation between the side rings is $6.581\,\mu$m. The straight waveguide and side rings have a refractive index of 3.5, while the central ring has a refractive index of 3.500491. This results in all three rings having an identical resonance frequency $\omega_o = 2\pi(193\text{THz})$ when the side ring detuning is $\Delta = 0$. The inter-ring coupling rate between the central ring and each side ring is $\kappa = 2\pi(17.9\,\text{GHz})$, the waveguide coupling rate is $\gamma_{\text{coup}} = 2\pi(18.7\,\text{GHz})$, and each ring has a very low amplitude-radiative loss rate of $\gamma_{\text{loss}} = 2\pi(38.6\,\text{MHz})$. The circles in Fig. 5 show the FDTD simulation results for the energy spectra $|a(\omega)|^2$ within the central ring at three different side ring detunings. Also shown in Fig. 5 are the spectras (solid lines) from the CMT model of the system [Eq. (6)] with identical values of the system parameters as in the FDTD simulations. Both the analytical CMT plots and FDTD simulation results show excellent agreement.

We next briefly comment on the spectras at the three different side ring detunings in Fig. 5: at zero detuning [Fig. 5(a)], the energy in the central ring is zero at its resonance frequency ω_o, and hence the system at this resonance frequency is at a *dark state* that is completely decoupled from the waveguide. When the side ring detuning Δ is non-zero [Fig. 5(b) and 5(c)], the spectrum of the energy in the central ring has a peak centered at its resonance frequency. In addition, the width of this peak increases as Δ is increased. This behavior is similar to varying the waveguide coupling rate in a single-ring system [Section 3] [12]. Namely, changing the waveguide coupling rate in the single-ring system also results in a variation of the resonator amplitude spectra width, while the peak center of the spectra stays fixed at the resonance frequency. This analogy suggests that varying the side ring detuning in Fig. 5 is similar to varying the effective waveguide coupling rate of the coupled-three-ring system.

The steady state analysis that was just presented motivates us to consider the possibility of modulating the system output by modulating the side ring detuning around the dark state. We next present a dynamical analysis of such a modulation process in a lossless coupled-three-ring system.

The modulation scheme we use in the following discussion involves a *push-pull* configuration where there is a π phase diferrence between the detunings $\Delta(t)$ of the side rings. This push-pull configuration can be shown to result in zero chirp in the output $S_{\text{out}}(t)$ [Eq. (6)] for an input $S_{\text{in}}(t)$ operating at the resonance frequency $\omega = \omega_o$. We note that a chirpless output is also a characteristic of a waveguide-coupling modulated single-ring system [Eq. (2)]. We also specialize to a $\Omega = 2\pi(20\,\text{GHz})$ sinusoidal $\Delta(t)$ modulation:

$$\Delta(t) = \delta\omega \sin(\Omega t) \tag{7}$$

where $\delta\omega$ is the resonance frequency modulation amplitude.

We numerically simulate the modulation process using the FDTD method. The FDTD simulation setup is identical to the setup for obtaining the central ring spectras in Fig. 5. We therefore operate in a non-adiabatic regime where the side ring detuning modulation rate Ω is comparable to the system coupling rates γ_{coup} and κ. Figure 6 shows the FDTD result (circles) of the system output power at $t \gg 1/\gamma_{\text{coup}}$ for the case of a CW input $S_{\text{in}}(t) = \exp(j\omega_o t)$ operating at the resonance frequency $\omega_o = 2\pi(193\text{THz})$ of the central ring, and a side ring modulation amplitude $\delta\omega = 2\pi(27.65\text{GHz})$ in Eq. (7). We emphasize that the time-averaged output optical power in Fig. 6 is equal to the time-averaged input optical power. In addition, the modulated output waveform is symmetrical with an infinite on/off ratio, and an output modulation frequency of 40 GHz that is twice the side ring modulation frequency. Also shown in Fig. 6 is the

#156102 - $15.00 USD Received 4 Nov 2011; revised 20 Jan 2012; accepted 30 Jan 2012; published 7 Feb 2012

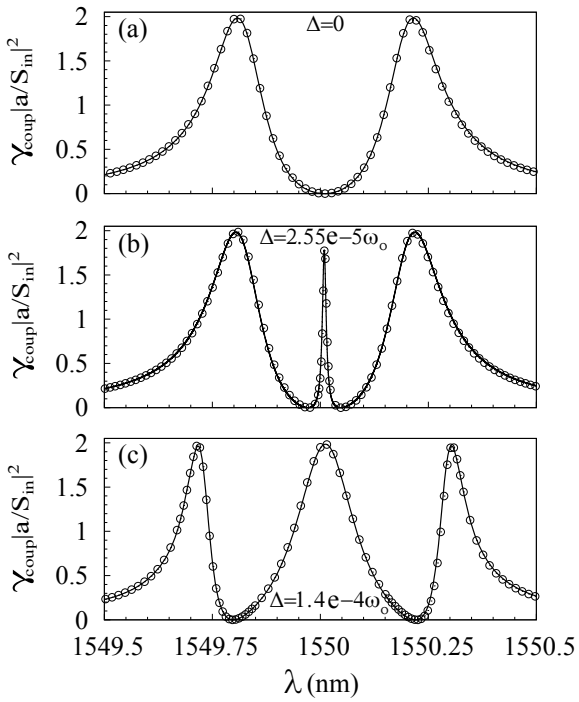

Fig. 5. Plots of the normalized spectra of energy $|a(\omega)|^2$ of the central ring resonator in the coupled-three-ring system (Fig. 4) from both FDTD simulations (circles) and the CMT model (solid line). The three spectras are at different side ring detunings Δ.

result (solid line) from numerically solving the system's CMT equations [Eq. (6)]. The CMT simulation has identical values of the system paramaters as in the FDTD simulation, except for a slight adjustment of the side ring detuning modulation amplitude to $\delta\omega = 2\pi(26.3\text{GHz})$ in order to fit the FDTD results. We also note that the phase of $S_{\text{out}}(t)$ in Eq. (6) is zero at all times during the modulation.

We next provide a qualitative explanation of the modulated output waveform in Fig. 6 based on the CMT model [Eq. (6)] of the system. Similar to the dynamics of the single-ring system discussed earlier, the output amplitude $S_{\text{out}}(t)$ of the coupled-three-ring system (Fig. 4) is the interference between a direct-path amplitude and an indirect-path amplitude, where the latter amplitude is now a coupled-three-ring resonance assisted indirect-path amplitude. Starting from any maximum output point in Fig. 6, the modulated output power trajectory in half a modulation period consists of the following three characteristic states whose electric field plots are shown in Fig. 7: (a) a maximum output power state, (b) a dark state and (c) a zero output power state. The maximum output power state [Fig. 7(a)] occurs when the direct-path amplitude interferes constructively with the indirect-path amplitude, while the zero output power state [Fig. 7(c)] occurs when there is destructive interference between the two pathways. In between this maximum and zero output power states is the dark state shown in Fig. 7(b) where the central ring amplitude $a(t)$ is zero. At this dark state, the central ring is completely decoupled from the waveguide, and the system ouput consists of only the direct-path amplitude $[S_{\text{out}}(t) = S_{\text{in}}(t)]$.

We also note that the output envelope in Fig. 6 has a modulation rate that is double the side ring modulation rate Ω [Eq. (7)]: within one modulation period $2\pi/\Omega$ of the side ring detuning $\Delta(t)$, the coupled-three-ring system states at times $t = t_1$ and $t = t_2 = t_1 + \pi/\Omega$ are identical up

#156102 - $15.00 USD Received 4 Nov 2011; revised 20 Jan 2012; accepted 30 Jan 2012; published 7 Feb 2012

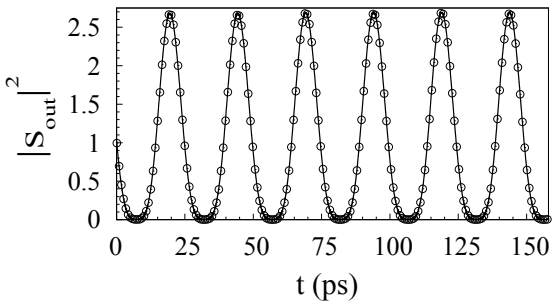

Fig. 6. Plot showing the 40 GHz modulated output power for the coupled-three-ring system (Fig. 4) at $t \gg 1/\gamma_{coup}$ from both CMT (solid line) and FDTD (circles) simulations. The side ring resonance frequency detuning $\Delta(t)$ is modulated at a frequency 20 GHz and amplitude $\delta\omega = 2\pi(27.65\text{GHz})$, while the other parameters are as follows: $\kappa = 2\pi(17.9\,\text{GHz})$, $\gamma_{coup} = 2\pi(18.7\,\text{GHz})$, $\omega_o = 2\pi(193\text{THz})$, and $S_{in}(t) = \exp(j\omega_o t)$.

to a flip in the sign of the detunings in both side resonators. Consequently, the system output has identical values at both times t_1 and t_2 within a modulation period, resulting in two identical output pulses for every one modulation cycle of the side ring detuning. This frequency doubling can be avoided by using a modulation $\Delta(t)$ in Eq. (6) that is always positive, for example.

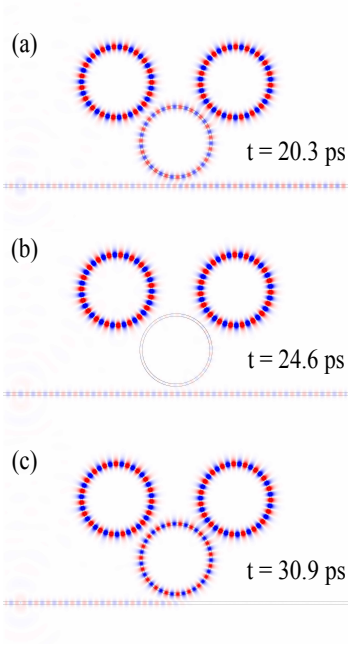

Fig. 7. Coupled-three-ring system electric field plots from FDTD simulations around the (a) maximum output power state, (b) dark state, and (c) zero output power state in Fig. 6. The electric field is polarized normal to the page.

#156102 - $15.00 USD Received 4 Nov 2011; revised 20 Jan 2012; accepted 30 Jan 2012; published 7 Feb 2012

5. Conclusion

In this paper, we presented a dynamical analysis of lossless modulation in two different resonator geometries: a single-ring system and a coupled-three-ring system. In both geometries, we demonstrated modulation schemes that result in a symmetrical output with an infinite on/off ratio. Both systems behave as lossless intensity modulators where the time-averaged output optical power is equal to the time-averaged input optical power. Although we only considered ring resonators with negligible intrinsic loss, the addition of intrinsic loss to the resonators results in little loss of optical power during the modulation process, as long as the resonator intrinsic loss rate is much smaller than the coupling rates of the system. For example, for a ring resonator with intrinsic loss rate of $\gamma_{\text{loss}} = 0.65\text{GHz}$ [20], both systems can be designed to have a time-averaged output optical power that is $> 90\%$ of the time-averaged input optical power.

In the coupled-three-ring system, lossless output modulation was achieved by performing push-pull modulation of the side ring detuning $\Delta(t)$ around the dark state of the system. In our numerical simulation example (Fig. 6), modulation of $\Delta(t)$ requires a fractional refractive index tuning of $\sim 10^{-4}$ which can be implemented using free carrier injection/depletion in silicon [20–22]. Ref. [22] also includes an example implementation for modulating the two side rings in parallel within a simple integrated circuit that allows for fast modulation of the side ring detuning.

Acknowledgments

The simulations were performed at the Pittsburgh Bigben Supercomputing Center and at the San Diego Trestles Supercomputer Center.

#156102 - $15.00 USD Received 4 Nov 2011; revised 20 Jan 2012; accepted 30 Jan 2012; published 7 Feb 2012